The Effect of Porous Data Surface Shape and Size on Ship Noise Prediction using the FWH Acoustic Analogy with Incompressible Solver for a

7th International Symposium of Marine Propulsors
smp'2022, Wuxi, China, October 17-21, 2022

The Effect of Porous Data Surface Shape and Size on Ship Noise Prediction using the FWH Acoustic Analogy with Incompressible Solver for a Cavitating Propellers

Marko Vikström[1], Urban Svennberg[1], Muye Ge[2], Rickard E. Bensow[2]

[1]Kongsberg Maritime Hydrodynamic Research Centre, Kristinehamn, Sweden

[2]Department of Mechanics and Maritime Sciences, Chalmers University of Technology, Gothenburg, Sweden

ABSTRACT

Using Ffowcs-Williams and Hawkings (FWH) acoustic analogy with an incompressible solver has become a rather common approach for ship noise prediction. Here the method is studied for a model scale container vessel. The numerical study includes both the ship hull and a rotating propeller, using the sliding mesh approach. The simulations are performed for a condition with cavitation around the tip of the propeller blades to study the propeller induced noise including the contribution from cavitation. To complement this study, e.g., to exclude any wall reflections and rotating sources, an additional pure monopole source case study was performed with both incompressible and compressible methodology. Since cavitation is a volume source acoustic term there is a need to use a Porous Data Surface (PDS) in combination with the FWH acoustic analogy. The choice of PDS shape and size using FWH is studied both for the model scale container vessel as well as for the pure monopole source case.

The results show that when using different PDS shapes, a directionality effect is evident when using the incompressible solver. The Sound Pressure Level (SPL) is dependent on the receiver angular location in relation to the PDS. The directionality effect is largest for a PDS shape where there is a large variation in distance from the source to the PDS faces, e.g. box. Furthermore, there is also a receiver distance discrepancy for the incompressible solver with FWH. The SPL curves for different receiver distance do not coincide for higher frequencies. Using a compressible solver and FWH, the shape effect and receiver distance discrepancy is not present.

Keywords

Ffowcs-Williams and Hawkings acoustic analogy, Incompressible flow, Compressible flow, Porous data surface, Directionality

1 INTRODUCTION

The appearance of cavitation on a marine propeller can be directly related to many negative side effects and the Underwater Radiated Noise (URN) by ships has been drawing more and more attention with increasing concerns of environmental impacts (Duarte, et al., 2021; Frisk, 2012). For full scale ship noise measurements, typically the vessel is tested in the open sea and a single or multiple hydrophone(s) with different possible deployments at far-field (typically at least 1-2 times of ship overall length) are used to collect the noise measurements. The Sound Pressure Level (SPL) measured by the hydrophone(s) will be corrected and scaled to the noise source level (Ls) equivalent at 1 m distance using formulations based on distance normalization of spherical spreading or similar. The resulting Ls are usually presented in 1/3 octave band spectrum and according to classification rules by ship classification societies, the Ls should be below certain thresholds. There are also recommendations and guidelines for the experimental noise measurement of model scale ships (ITTC7.5-02-01-05, 2017). The model scale ship and propeller can be tested inside a large-size cavitation tunnel and the transmission loss (TL) can be measured as the noise propagation loss inside the confined space of the cavitation tunnel test section.

The efforts to do numerical predictions for marine propeller induced noise have increased considerably in recent years, with many investigating the use of acoustic analogies, such as the Ffowcs Williams-Hawkings (FWH) approach for these hydrodynamic flows.

Incompressible simulation has been used for the prediction of ship hydrodynamics and cavitation dynamics with satisfying predictions including induced near-field pressure fluctuations and hull pressure pulses (Ge, Svennberg, & Bensow, 2020) and numerical prediction of

ship radiated noise with the combination between incompressible simulation and FWH acoustic analogy for ships with cavitating propeller has been investigated including (Li, Hallander, & Johansson, 2018). But this combination with the usage of incompressible solution might be erroneous as reported in the study in (Ahmed, 2020) by the comparison between incompressible and compressible LES with FWH acoustic analogy. In our earlier work in (Ge, Svennberg, & Bensow, 2022), results also indicate the combination between incompressible flow input and FWH acoustic analogy can be erroneous.

In the present study, the flow predictions using an incompressible solver are provided as input for the FWH acoustic analogy on several defined Permeable Data Surfaces (PDS), consisting of sets of spheres, cylinders and boxes, to predict a model scale ship generated under water noise. The results show that with the combination of incompressible flow input and the PDS-FWH approach, the noise predictions are dependent on the shape of the PDS as well as receiver placements. Significant spreading can be found between different combinations of PDS and receiver locations with unrealistic noise directivities.

2 NUMERICAL METHOD

The commercial package STAR-CCM+ was used to perform numerical simulations with the incompressible single fluid homogeneous mixture approach representing the two phases of liquid and vapor. Mass transfer is modelled by the Schnerr-Sauer model and turbulence is modelled using RANS approach with $k-\omega\ SST$ turbulence model.

The noise predictions are achieved via 'on the fly FWH' noise prediction in Star-CCM+ with the FWH acoustic analogy with input from the incompressible simulations. The FWH equation rearranges the continuity and the momentum equations into the form of an inhomogeneous wave equation and was proposed in (Williams, 1969) considering impermeable surfaces in motion, referred to as S-FWH,

$$\square^2 p' = \frac{\partial}{\partial t}[\rho_0 v_n \delta(f)] - \frac{\partial}{\partial x_i}[p n_i \delta(f)] + \frac{\partial^2}{\partial x_i \partial x_j}\left[H(f) T_{ij}\right], \quad (1)$$

in which $\square^2$ represents the D'Alembert operator, n represents the unit outward normal of the surface, v_n represents the local normal velocity of the surface, p represents the local gage pressure on the surface and T_{ij} represents the Lighthill stress tensor defined as

$$T_{ij} = \rho u_i u_j - \sigma_{ij} + (p' - c^2\rho')\delta_{ij},$$

in which δ_{ij} represents the Kronecker delta and σ_{ij} is the viscous stress tensor. Formulating it with a porous data surface, it is referred to as PDS-FWH,

$$\square^2 p' = \frac{\partial}{\partial t}[\rho_0 U_n]\delta(f) - \frac{\partial}{\partial x_i}[L_i \delta(f)] + \frac{\partial^2}{\partial x_i \partial x_j}\left[H(f) T_{ij}\right],$$

$$U_n = \left(1 - \frac{\rho}{\rho_0}\right) v_n + \frac{\rho u_n}{\rho_0},$$

$$L_i = p\delta_{ij} n_j + \rho u_i (u_n - v_n).$$

The first term on the right-hand side in Equation (1) represents the thickness term and the second term represents the loading term; both terms are evaluated on the impermeable data surface $f = 0$ through the Dirac delta function $\delta(f)$. The third term represents the nonlinear quadrupole term outside the surface $f = 0$. With the PDS-FWH formation, the first two terms loses their physical meaning and referred to as pseudo-Thickness and pseudo-Loading terms and the PDS should ideally placed enclosing all the non-negligible quadrupole sources and the volume integration outside the surface is no longer needed. The Farassat formulation 1A (Farassat & Succi, 1980; Brentner & Farassat, 1998) for permeable data surfaces is used and implementation details in Star-CCM+ can be found in (Siemens, 2020).

3 SIMULATION SETUP

The presentation of results is shown in two parts. In the first part, the URN predictions of the model scale container vessel are presented focusing on prediction differences using varying shapes of permeable data surfaces using FWH. The second part represents a simplified but representative monopole case to further address the problematic URN predictions with incompressible flow input.

3.1 Configuration of the container vessel

The studied case is the container vessel used in the VIRTUE and SONIC EU project with main geometrical information summarized in **Table *1***.

Table 1 Main geometrical characteristics of the container vessel and the paired propeller.

Length between perpendiculars, Lpp	232.0 m
Beam, moulded	32.2 m
Draft at forward/aft perpendiculars	11.3 m
Displacement	50885.0 m3
Block coefficient, CB	0.602
Waterplane coefficient, CW	0.809
Propeller distance from after perpendicular	4.8 m
Number of propellers, NP	1
Propeller diameter, D	7.9 m
Pitch ratio 0.7R/D	1.109
Chord length at 0.7R	2.5 m
Propeller tip clearance	27.7% D

The model scale vessel was tested inside the large-size cavitation tunnel HYKAT by HSVA with scale ratio (λ) of 29.1. The size of the test section is 11 m × 2.8 m × 1.6 m, with a fixed propeller rotation speed of 28 rps. In the simulation, instead of the tunnel test section, a domain size of 24 m × 5 m × 5 m is used. It can be noted that a larger domain with non-reflecting boundary conditions are desired for compressible simulations to avoid acoustic wave reflections; but in the present study the incompressible approach is used without actual existence of acoustic waves, thus a moderate sized domain is used to avoid blockage effect and outer boundary effect around the ship (where PDS will be defined) which also save computational resources comparing to a very large one. Symmetry plane boundary condition is used to replace the free-surface and the other sides of the domain. The thrust coefficient K_T and cavitation number σ were matched to the experimental value K_T = 0.2354 and σ=0.2234, with inlet velocity adjusted to 7.43 m/s and the same propeller rotation speed 28 rps. Three individual simulations with were carried out for each shape of PDS.

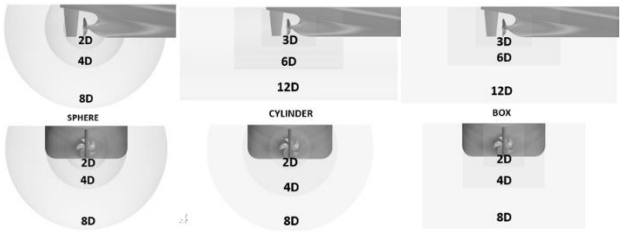

Figure 1 PDS-FWH sizes and shapes for the container vessel case

To collect flow information for the PDS-FWH predictions, 3 PDS sizes are used for each shape, i.e. Sphere, Cylinder and Box, as shown in **Figure *1***. Hereafter for all the shape types, the sizes is denoted by 2D, 4D and 8D respectively. The computational domain has in total about 100 million cells, with 47 million in the sliding mesh domain of the propeller which are identical for all three cases. The smallest size for the tip vortex mesh resolution is about 0.1mm, and the refinement mesh size for the largest PDS-Shape, i.e. 8D volume is 0.01m and it follows the shape of the PDS. The identical propeller meshes and the mesh size definition in the outer domain will assure similar wake dynamics, thus also cavitation dynamics for the three cases. Moreover, this also in combination with the matching conditions describes above for K_T and σ.

In **Figure *2***, the outline of the hydrophone position for the radius of 4.2m for 2 planes are shown, symmetry and propeller plane respectively.

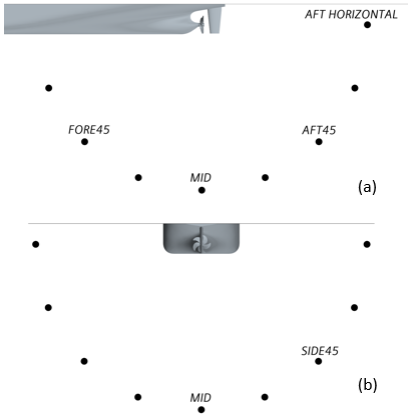

Figure 2 Outline of hydrophone positions at 4.2m in (a) symmetry plane and (b) propeller plane

There are in total 8 planes for different azimuthal angle with 22.5 ° increments and for 3 different radius 2.4m, 100m and 1000m respectively. This will in combination with PDS shapes and sizes end up in 1566 unique evaluation positions for the hydrophones.

The timestep chosen to correspond to 2048 increments per propeller revolution speed, i.e. about 0.176 degrees per timestep for the propeller rotation. A second-order implicit time advancing scheme was used. When the developed cavitation dynamics pattern was achieved additional 5 propeller revolutions for the FWH analysis was carried out. All the simulations use the double precision version of Star-CCM+.

3.2 Configuration of the monopole test case

A stationary standalone monopole source generating noise in free space, as shown in **Figure 3**, is set up. The mass rate of the volume meshed spherical monopole source is derived from simulations of the model scale vessel, i.e. the first order derivative of the predicted integrated total vapor volume with radius a = 0.01 m as $\rho_{water}\frac{\partial V_{vapor}}{\partial t}/(4/3\pi a^3)$ plotted in **Figure 4**. The volume of the designed monopole is about 4.2 cm^3 which is similar in size to the total vapor volume in the vessel simulation which is about 3.0 cm^3. The computational domain is very large with a cubic box with an edge length of 260 m. The simulations were run for 0.07s, approximate to the time of 2 propeller revolutions with data collection for the second revolution time. Several PDS were defined for noise prediction using FWH, denoted to PDS-ML1 to PDS-ML4 shown in **Figure 3**. Both compressible and incompressible simulations are performed. For the compressible simulation, there is no special treatment on the outer boundaries as the domain is large enough to avoid possible reflections influencing the results during this limited simulation time. For the incompressible simulation, the six outer patches are set to mass flow input boundaries with mass flow calculated based on the input monopole source, to guarantee mass conservation in the simulation domain. There are in total 18.8 million cells for the computational grid with the maximum target cell length of 0.02 m inside PDS-ML4.

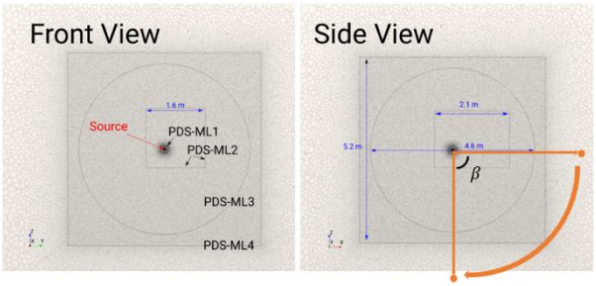

Figure 3 The free-field monopole with PDS-FWH placements.

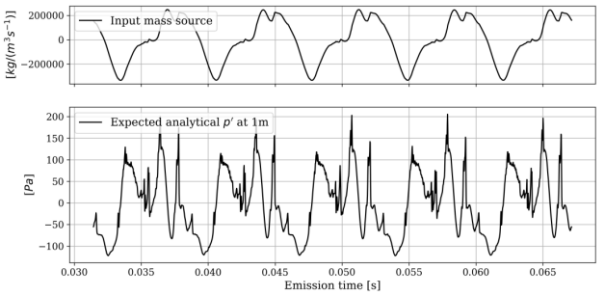

Figure 4 Input mass source and expected analytical p' at 1 m distance.

4 RESULTS AND DISCUSSIONS

4.1 The container vessel

According to the derivation of FWH for compressible simulations the size and shape of the PDS does not affect the result when all sources of importance are included inside the PDS and the mesh resolution inside it is sufficient. (Ge, Svennberg, & Bensow, 2022) have shown that this is not the case when FWH is applied to incompressible simulations. **Figure *5***, show the source level SPL calculated from all the 1566 hydrophones included in the simulation. It is clear from the figure that there is a huge spread in the predicted source level for all frequencies, especially for the higher frequencies, thus the shape and size as well as the location for the hydrophone has a huge impact on the predicted SPL source level. A selection of curves is presented below to get a better understanding of the reason for the huge spread in the results.

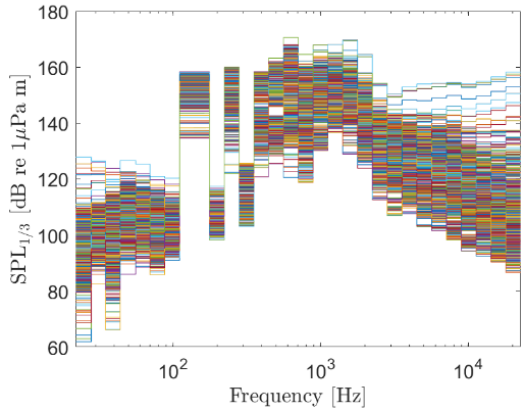

Figure 5 Source level SPL for all the receivers in combination of all PDS shapes and sizes

The first peak above 100 Hz corresponds to the blade frequency and is dominated by the displacement of the water from the thrust of the blade. The second peak is two times the blade frequency and comes from the blade passage through the wake but is modelled and strengthened by the sheet cavitation on the blade. The mid frequency hump, centered around 1000 Hz, is generated by the tip vortex cavitation and its interaction with the sheet cavitation on the tip of the blade. The center frequency and level of this hump is important in many noise classifications.

Figure *6*, shows nine curves for the hydrophones in the arch in the propeller plane, shown in **Figure *2*** (b), for the hydrophones placed 100 m from the propeller center listening to the 4D PDS. These curves are low frequency cut at 100 Hz since there is not much interest in the low levels below the blade frequency, the first peak above 100 Hz covers the blade frequency. The curves for the sphere PDS are rather similar to each other. However, there is a small spread. This can come from that the main source for pressure fluctuations here is the cavitation around the top position for the blades and the PDS is centered around the propeller center. Thus, there is a difference in distance from the cavitation to the PDS in different directions. The curves for the cylinder PDS, in **Figure *6***, has a similar spreading as the curves for the sphere but with higher values at the highest frequencies.

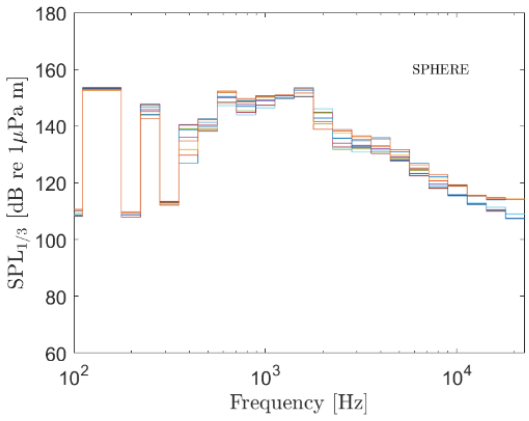

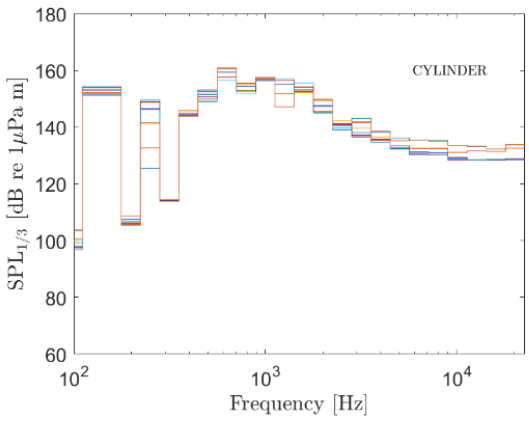

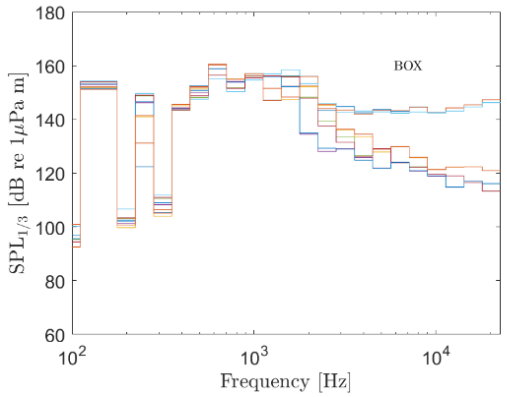

Figure 6 Source level SPL for different shaped PDS with the size of 4D and the distance 100 m in the propeller plane

The hypothesis is that since there is no phase shift/ time delay for the pressure fluctuations at different locations on the PDS due to the infinite speed of sound in incompressible simulations. The spatial distribution of predicted noise levels indicates that the PDS transmits waves of the same shape as the PDS. The sphere looks the same no matter the viewing direction, thus, similar waves are transmitted in all directions. The cylinder also has the same shape irrespective of viewing direction in the propeller plane but in contrast to the sphere there is a line of cells pointing towards the hydrophone in this case. The curves for the box, in **Figure *6***, strengthen the hypothesis. The two curves with highest values at the high frequencies are for the hydrophone straight below the propeller and the two at the sides, all facing a big flat surfaces of the box PDS. The two lowest curves are the curves for the hydrophones at 45 degrees, facing the corners of the box PDS. This is not clear to the reader since there is no legend included in the figure, but it can be seen in **Figure *8*** below. The reason to why the differences are more pronounced for the higher frequencies is that if a transmitting surface is larger than the wavelength it will give a directivity to the transmitted waves. The bigger the surface is the more directivity is given to the waves.

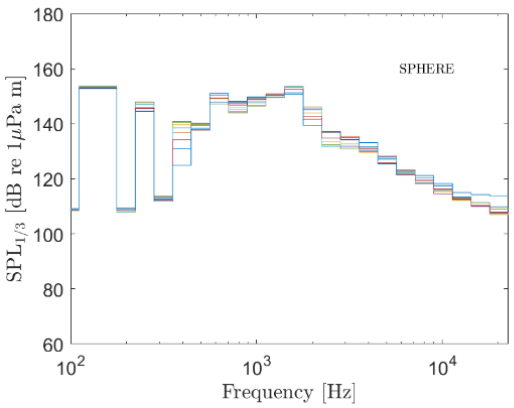

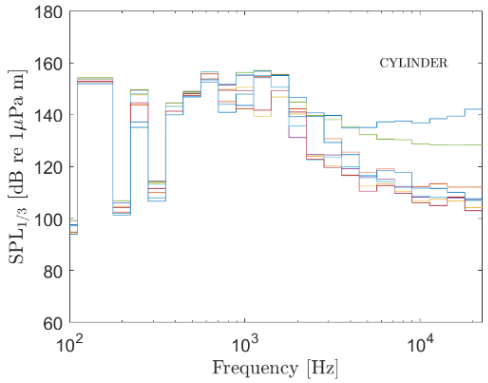

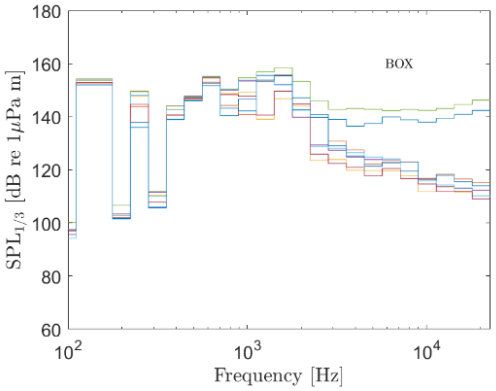

Figure 7 Source level SPL for different shaped PDS with the size of 4D and the distance 100 m in the symmetry plane

The box PDS here is about 1 m wide and 1.5 m long which corresponds to 1500 Hz and 1000 Hz respectively. It can be seen in **Figure *6***, that the curves start to deviate from each other at about 1000 Hz.

Figure *7* shows eight curves for the hydrophones in the arch in the symmetry plane along the center line of the hull, shown in **Figure *2*** (a).The curves for the sphere PDS, in **Figure *7***, are similar to the curves for the propeller plane in **Figure *6***. The curves for the cylindrical PDS, in **Figure *7***, differ from the curves in the propeller plane in **Figure *6***, and are here similar to the curves for the box PDS, in **Figure *6*** and **Figure *7***. The curve with highest values at the higher frequencies is for the hydrophone aft of the propeller which is facing the flat end surface of the cylinder, the second curve is the one below the propeller. The curves for the box PDS, in **Figure *7*** are similar to the curves in **Figure *6***. The main observation here is that there is a larger difference between the two curves with highest value compared to **Figure *6***. This comes from that the end surface of the box is smaller than the side and bottom sides of the box which results in slightly lower values for the hydrophone aft of the propeller.

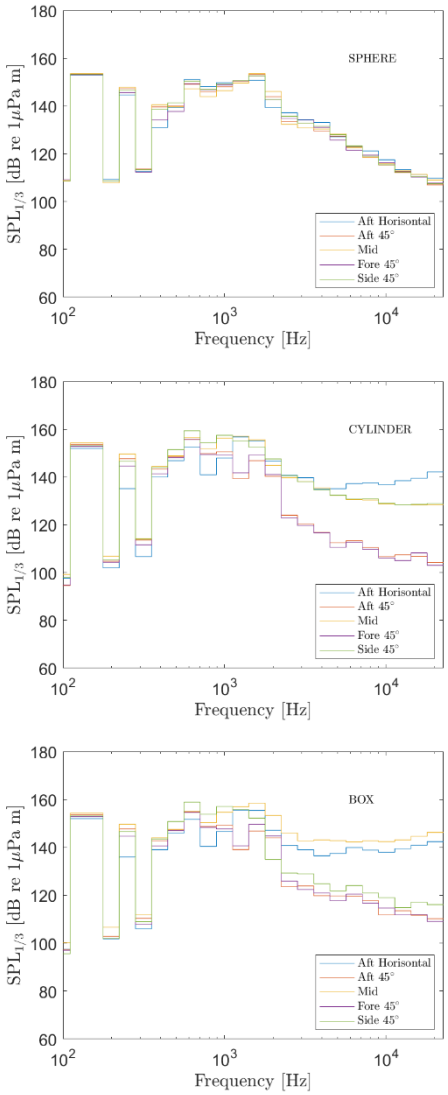

Figure 8 Source level SPL for different shaped PDS with the size of 4D and the distance 100 m for the 5 points marked in Figure 2

Figure *8* shows the source level SPL curves for the five hydrophone locations named in **Figure *2***, at 100 m away from the propeller center. With the lower number of curves in each figure it is possible to add the legend and see which hydrophone that is connected to each curve. The curves for the sphere PDS here, in **Figure *8***, are also present in **Figure *6*** and **Figure *7***, and do not show any significant differences due to direction. The discussion above for the cylinder PDS is here, in **Figure *7***, confirmed by that the curve with the highest high frequency SPL source level in the hydrophone aft of the propeller facing the flat end surface of the cylinder. Below this curve there are two curves for hydrophones facing the side of the cylinder, Mid and side 45 °, with significantly higher SPL values then for the sphere PDS. The curves for the box PDS, in **Figure *8***, also confirm the analysis above that the high frequency SPL levels are higher for the hydrophones facing flat surfaces of the PDS and lower levels for the hydrophones facing the corners of the PDS.

4.2 The monopole test case

There are 10 noise receivers to collect acoustic predictions on the x-z plane, as demonstrated in **Figure 3** in orange color. All the receivers have the same distance d = 1000 m to the designed monopole source located at the center of the x-z plane, with the angular position β varying from 0 degrees to 90 degrees with 10 degrees interval.

With the block-shaped PDS-ML2, the predicted acoustic source levels at different receiver locations are shown in **Figure *9***. It can be seen clearly that the predicted noise levels show strong directivity with unrealistic high levels, especially at higher frequencies. For the present designed monopole case, it is known to be omnidirectional and furthermore, as shown in **Figure *11*** and **Figure *12***, with the compressible flow input both PDS-ML2 and PDS-ML3 predict the source SPL in agreement with expected analytical solution. Using the spherical PDS-ML3 the predictions also show no directivity shown in **Figure *10*** and generally agree with the expected analytical solution, with noticeable under-predictions at the 1st BPF.

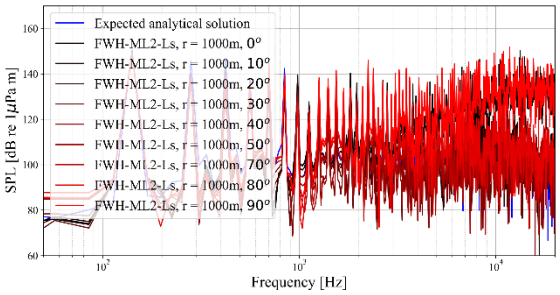

Figure 9 Predicted source SPL using different receiver locations; incompressible input on PDS-ML2

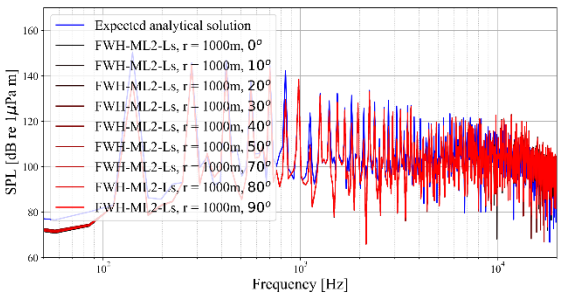

Figure 10 Predicted source SPL using different receiver locations; incompressible input on PDS-ML3

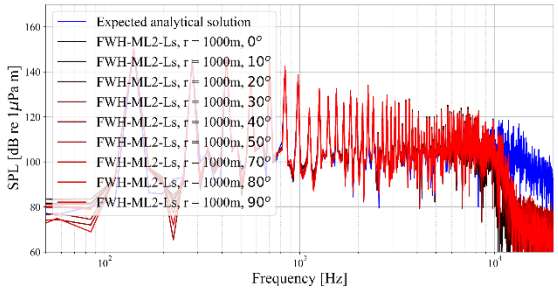

Figure 11 Predicted source SPL using different receiver locations; compressible input on PDS-ML2

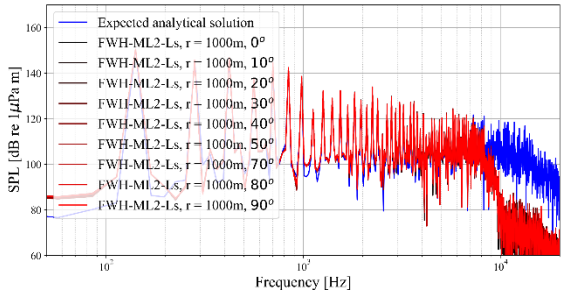

Figure 12 Predicted source SPL using different receiver locations; compressible input on PDS-ML3

These results show there may be two problems using incompressible flow input together with the FWH acoustic analogy. The first one is the prediction dependency with the shape of the PDS: block PDS predicted different source SPL compared with a spherical PDS for a standalone monopole case and unrealistically high levels of noise are predicted at higher frequencies with strong directivities. The explanation is the lack of sound wave traveling time from the source to the PDS using an incompressible solver where pressure affect the PDS simultaneously. The second one is that using an incompressible solver with a source centered spherical PDS, even though there is no directivity nor high frequency over predictions, the noise levels at certain frequencies, especially noticeably at BPF, are under-predicted. This can be related to the velocity prediction differences between an incompressible solver and a compressible solver, again due to lack of a propagating wave.

Using an incompressible solver, the predicted pressure is hydrodynamic pressure and based on the present configuration the expression can be derived using unsteady Bernoulli equation

$$p' = p_0 + \frac{\rho}{4\pi r}\frac{\partial Q(t)}{\partial t} - \frac{1}{2}\rho\frac{Q(t)}{(4\pi r^2)^2},$$

in which the last term is very small. For a free-field monopole, the predicted $p'$is acoustic pressure and can be derived as

$$p' = p_0 + \frac{\rho}{4\pi r}\frac{\partial Q(t - r/c_0)}{\partial t},$$

which is similar to the incompressible hydrodynamic pressure expression with time delay r/c_0 from the source to the receiver. The comparison between predicted pressure fluctuation at 2 m away from the designed monopole source are shown in **Figure 13** and **Figure 14**.

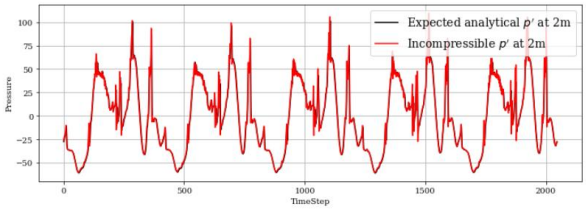

Figure 13 Predicted incompressible pressure at 2m distance.

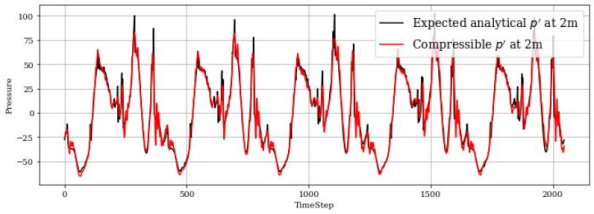

Figure 14 Predicted compressible pressure at 2m distance

The predicted pressures at 2 m distance are very similar between an incompressible solver and a compressible one, but the velocities are predicted differently. For the incompressible solver, the velocity fluctuation can be expressed using simply mass conservation law resulting to

$$U'(r,t) = \frac{1}{4\pi r^2}Q(t),$$

and for the monopole case the velocity fluctuation can be expressed as

$$U'(r,t) = -\frac{1}{4\pi}\frac{\partial}{\partial r}\frac{Q\left(t - \frac{r}{c_0}\right)}{r}.$$

The predicted velocity fluctuations using the incompressible and the compressible solver, together with comparison to the analytical solutions are shown in **Figure 15** and **Figure 16**. Note that the shown results are based on a receiver at 2 m distance to the source; the difference between incompressible and compressible velocity fluctuations are much smaller if considering a receiver at 0.2 m, indicating the FWH prediction discrepancies are significant using incompressible input with large sized PDS and might be small using a small size PDS.

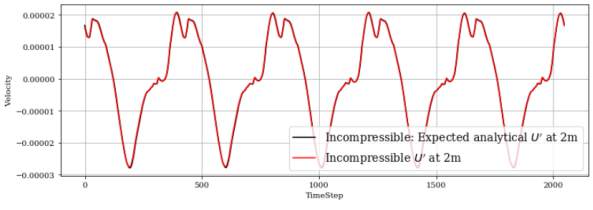

Figure 15 Velocity fluctuations using the incompressible solver

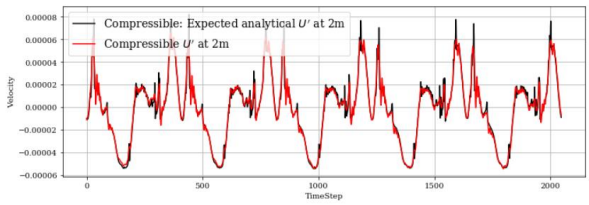

Figure 16 Velocity fluctuations using the compressible approach

5. CONCLUSIONS

The main conclusion presented here is that when using incompressible simulations as a base for FWH analysis the infinite speed of sound makes the entire PDS to transmit waves where all surfaces of the PDS is in phase with each other. This result in transmission of waves which is strongly influenced by the shape of the PDS. Furthermore, if the PDS is large compared to the wavelength of the transited waves the predicted SPL source level will become dependent on the distance between the hydrophone and the PDS. It seems the artificial directivity can be relatively small for a centered monopole source with a spherical PDS. But a spherical PDS is hard to accomplish in a case with a cavitating propeller where the cavitation is moving with the rotation of the blade and is larger for some blade positions then other positions.

REFERENCES

Ahmed, S. (2020). On the noise generated by a ship propeller. University of New South Wales.

Brentner, K., & Farassat, F. (1998). Analytical Comparison of the Acoustic Analogy and Kirchoff Formulation for Moving Surfaces. AIAA Journal, 1379-1386.

Duarte, C. M., Chapuis, L., Collin, S. P., Costa, D. P., Devassy, R. P., Eguiluz, V. M., . . . others, a. (2021). The soundscape of the Anthropocene ocean. Science.

Farassat, F., & Succi, G. P. (1980). A review of propeller discrete frequency noise prediction technology with emphasis on two current methods for time domain calculations. Journal of Sound and Vibration, 399--419.

Frisk, G. V. (2012). Noiseonomics: The relationship between ambient noise levels in the sea and global economic trends. Scientific reports, 1--4.

Ge, M., Svennberg, U., & Bensow, R. (2020). Investigation on RANS prediction of propeller induced pressure pulses and sheet-tip cavitation interactions in behind hull condition. Ocean Engineering, 107503.

Ge, M., Svennberg, U., & Bensow, R. (2022). Investigations on prediction of ship noise using the FWH acoustic analogy with incompressible flow input. Ocean Engineering.

ITTC7.5-02-01-05. (2017). Model-scale propeller cavitation noise measurements. ITTC Quality System Manual, Recommended Procedures and Guidelines.

Li, D.-Q., Hallander, J., & Johansson, T. (2018). Predicting underwater radiated noise of a full scale ship with model testing and numerical methods. Ocean Engineering, 121--135.

Siemens. (2020). Simcenter STAR-CCM+ User Guide. Simens Digital Industries Software.

Williams, J. F. (1969). Sound generation by turbulence and surfaces in arbitrary motion. Philosophical Transactions for the Royal Society of London. Series A, Mathematical and Physical Sciences, 321--342.